ACS OMEGA

Open Access

http://pubs.acs.org/journal/acsodf

Article

Phononic Stiefel–Whitney Topology with Hinge Vibrational Modes in 3D Carbon Allotrope 4^3T57-CA

Yang Li*

Cite This: *ACS Omega* 2024, 9, 46610–46614

Read Online

ACCESS | Metrics & More | Article Recommendations | Supporting Information

ABSTRACT: As a fragile topological state lacking spin–orbit coupling (SOC) and possessing space–time inversion (*PT*) symmetry, the Stiefel–Whitney (SW) insulator has received much attention. Up until now, the identification of SW insulators has been extensively suggested for 2D phononic systems but has been rarely considered for 3D phononic systems. 3D carbon allotrope 4^3T57-CA has the capability to achieve nontrivial phononic SW topology, which can be distinguished by a nontrivial second SW number. Moreover, 3D 4^3T57-CA can host hinge vibrational modes, which are protected by *PT*.

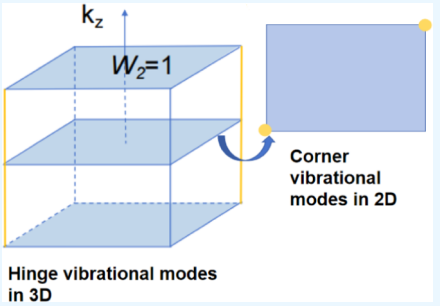

INTRODUCTION

There has been significant interest in condensed matter research due to the unique topological states[1−5] of matter and their material realization. Broadly speaking, four characteristic classes exist: the Chern class, SW class, Pontryagin class, and Euler class. Among them, the SW class[6,7] originated in the mathematical structure of the *real*-valued vector bundles associated with the *real*-valued wave functions. SW insulators,[8−13] belonging to the SW class, are distinguished by the existence of *real* band eigenstates, which are ensured by specific symmetries, such as *PT*, and the lack of the SOC effect.

From a strict perspective, SOC is unavoidable in electronic materials. Consequently, the requirement for spin–orbit-free conditions, which is a demanding criterion for electronic SW insulators, can be naturally circumvented in phononic systems due to the absence of spin in phonons.[14−20] It is important to mention that starting in 2010, the application of research on the Berry phase and topological physics led to the emergence of a new area called *topological phononics*,[21−25] which focuses especially on the study of phonons.

Very recently, 2D phononic SW insulators[12,26−29] have received significant attention from researchers. For example, Pan and Huang[12] predicted that 2D Xenes and their ligand-functionalized derivatives are possible candidates with phononic SW topology and corner vibrational modes. Mu et al.[27] proposed that 2D graphdiyne with a Kekulé lattice can cohost phononic and electronic SW topology. Zhu et al.[28] found that the phonons in 2D graphdiyne and γ-graphyne exhibit an SW topology and suggested a method to achieve 3D phononic SW insulators in 3D graphdiyne. Nevertheless, there is currently a scarcity of suitable materials for 3D phononic SW insulators, which presents a significant obstacle to performing follow-up research on the phononic physics related to the SW class.

This work reveals the SW topology in the 3D carbon allotrope 4^3T57-CA proposed by Blatov et al.[30] using a high-throughput screening method. The designation of carbon allotrope 4^3T57-CA (or 4,4,4T57-CA) indicates that this hypothetical carbon allotrope consists of three distinct 4-coordinated atoms, exhibits 3-fold periodicity, and is ranked 57th among a group of other hypothetical carbon allotropes with the same number of distinct four-coordinated atoms and 3-fold periodicity. We would like to emphasize that the 3D SW topological phase has been reported to exist in artificial systems, including 3D acoustic nodal-line crystals,[31] which belong to artificial composite systems. However, our work mainly focuses on 3D crystalline phononic materials belonging to solid-state systems. In 2024, Xu et al.[32] contributed to the catalog of topological phonon materials, they studied the topological states in more than 10 000 3D crystalline phononic materials and investigated the phononic boundary states in these materials. For the phononic boundary states, they only focused on the case of phononic surface states, and the phononic hinge states in 3D crystalline phononic materials with SW topology have not been studied. Our work can be viewed as a new research point to study the coexistence of the rich phononic boundary states (i.e., 2D surface and 1D hinge states) in 3D crystalline phononic materials. The nontrivial SW topology in 3D 4^3T57-CA can be verified by computing the w_2[33−38] of the phononic gap in the phononic dispersion curves. Additionally, the nontrivial w_2 manifests as topological boundary

Received: September 29, 2024
Revised: October 22, 2024
Accepted: October 25, 2024
Published: November 4, 2024

modes located at a pair of *PT*-symmetric hinges of a nanotube sample of 4^3T57-CA. This makes 3D 4^3T57-CA an excellent platform for studying the phononic SW topology with hinge vibrational modes.

METHODS

The calculations in this work were carried out within the framework of density functional theory by using the Vienna Ab initio Simulation Package.[39] The Perdew−Burke−Ernzerhof[40] functional with generalized gradient approximations[41] was adopted to describe the exchange−correlation interactions. The computations were conducted using a plane-wave cutoff of 500 eV. The convergence criterion for the electronic self-consistency loop was established at 10^{-6} eV on the 9 × 9 × 1 Monkhorst−Pack *k*-point mesh. In terms of structural relaxation, the Hellmann−Feynman forces acting on each atom were assumed to be −0.01 eV/Å. To assess dynamic stability, phonon spectra were calculated using the density functional perturbation theory implemented in the PHONOPY program.[42]

Figure 1a shows the relaxed crystal structure of the 3D carbon allotrope 4^3T57-CA with a *P*21/c space group (number 14)

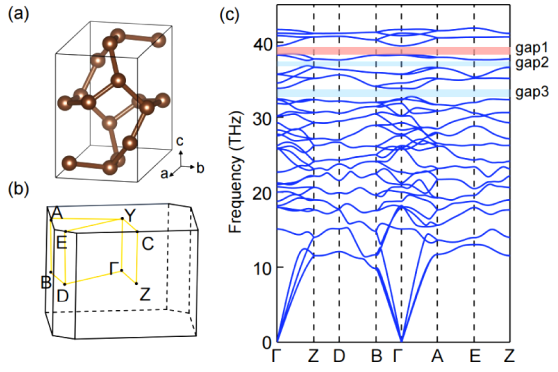

Figure 1. (a) Optimized crystal structures for the 3D 4^3T57-CA. (b) 3D Brillouin zone (BZ). (c) Phononic dispersion curves for 3D 4^3T57-CA. Three phononic gaps (gaps 1−3) are apparent.

generated by inversion and 2-fold rotation symmetries. The three C atoms occupy the 4*e* Wyckoff position, as listed in Table 1. Based on the fully relaxed structure, the obtained lattice

Table 1. Structural Parameters of 3D 4^3T57-CA

atoms	Wyckoff position	*x*	*y*	*z*
C	4*e*	0.32768	0.02299	0.98507
C	4*e*	0.20170	0.32049	0.74359
C	4*e*	0.08327	0.63268	0.90056

parameters are a = 4.37813 Å, b = 3.42706 Å, and c = 5.02108 Å, which are in good agreement with the data exhibited in SACADA[43] (a = 4.36440 Å, b = 3.41330 Å, and c = 5.00400 Å). For the phononic bands of 3D 4^3T57-CA, the SOC could be ignored. That is to say, the phonon system of 3D 4^3T57-CA possesses $PT^2 = 1$.

The phononic dispersion curves can be used to evaluate the dynamic stability of 3D 4^3T57-CA. Figure 1c demonstrates the absence of imaginary frequencies in the phononic dispersion curves along the selected symmetry paths, confirming the dynamic stability of 3D 4^3T57-CA. Then, the thermal stability of a 3 × 3 × 3 3D 4^3T57-CA was examined with the help of ab initio MD simulations[44] within the canonical ensemble (NVT) at 300 K, for 3000 fs (i.e., 3 ps) with a time step of 1 fs. The relationship between the total energy and the time at 300 K is given in Figure S1. One finds that 4^3T57-CA can maintain its stable structure at 300 K because its total energy fluctuation is not large. Finally, we evaluate the mechanical stability of 3D 4^3T57-CA. The results are shown in the Supporting Information. The elastic constants of 3D 4^3T57-CA satisfy all of the criteria[45] listed in the Supporting Information, and therefore, the material is mechanically stable.

RESULTS AND DISCUSSION

Remarkably, three obvious phononic gaps (gaps 1−3) exist within the frequency range 30−40 THz. To examine if the hinge vibrational modes appear in these three gaps, we build a phononic tight-binding model for the 1D tube geometry of 3D 4^3T57-CA, preserving its *PT* symmetry. The TB model is generated based on the "FORCE_CONSTANTS" generated by DFPT calculations with the help of PhonopyTB code.[46] Subsequently, we perform the calculations of the phononic dispersion curves for the constructed nanotube (in the k_z direction). The results presented in Figure 2a reveal that the phononic dispersion curves of the nanotubes exhibit three gaps and no imaginary frequencies. In addition, for a better view of the phononic degenerate state, we also show the phononic spectrum of the constructed nanotube of 3D 4^3T57-CA at $k_z = 0$ in Figure 2b. Surprisingly, one finds that a boundary mode exists within phononic gap 3 of 4^3T57-CA (see Figure 2c). Moreover, the boundary mode (blue line in Figure 2c) has a double degeneracy (see the blue dots in Figure 2d) and does not connect the upper and lower phononic bands of phononic gap 3.

In Figure 3, we depict the spatial distribution of the doubly degenerate state at $k_z = 0$ as shown in Figure 2c,d, and one finds that the state is localized at one pair of *PT* symmetry-related hinges,[47−51] characterizing the properties of in-gap topological hinge modes in 3D phononic SW insulator.

Then, we come to understand the hinge vibrational modes within phononic gap 3 of 3D 4^3T57-CA by the w_2. To examine the SW topology of phononic gap 3, we assess the w_2 for a 2D slice of BZ with fixed k_z. Considering the system's global band gap, it can be inferred that all 2D k_z-slices are adiabatically connected, hence necessitating a shared w_2. One can select a particular slice, such as the $k_z = 0$ or $k_z = \pi$ plane, to determine the w_2.

In this work, the $k_z = 0$ plane is selected as an example, and the w_2[10] of it can be readily extracted from the parity eigenvalues at the four time-reversal invariant momentum (TRIM, labeled as Λ_i) points on $k_z = 0$ plane, with $(-1)^{w_2} = \prod_{i=1}^{4}(-1)^{[N_n^-(\Lambda_i)/2]}$.[12] The $\lfloor\cdots\rfloor$ is the floor function, and $N_n^-(\Lambda_i)$ is the number of occupied phononic bands below gap n (n = 3 here) with negative *PT* eigenvalue at TRIM Λ_i.

The results of w_2 for $k_z = 0$ are exhibited in Table 2. As shown in Table 2, at the Γ point, 12 occupied phononic bands exhibit positive parity eigenvalues and 14 occupied phononic bands exhibit negative parity eigenvalues. By comparison, 14 occupied phononic bands exhibit positive parity eigenvalues at the *X* point, and 12 occupied phononic bands exhibit negative parity eigenvalues. The mismatch $N_3^-(\Gamma) - N_3^-(X) = 2$ signals a double band inversion, reflecting a nontrivial topology.

As shown in Figure 4, each 2D k_z plane can be viewed as a 2D phononic SW insulator, which has the doubly degenerate state

https://doi.org/10.1021/acsomega.4c08904
ACS Omega 2024, 9, 46610−46614

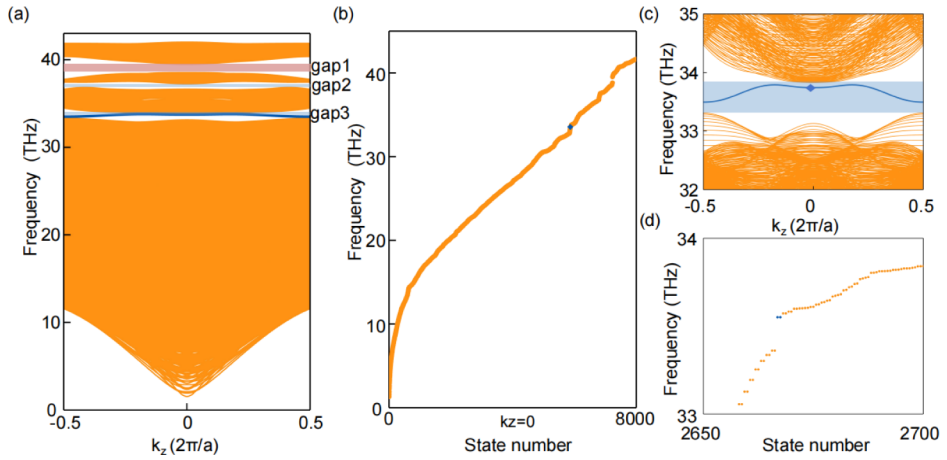

Figure 2. (a) Phononic dispersion curves of the nanotube (in the k_z direction). (b) Phononic spectrum of the nanotube at $k_z = 0$. (c,d) Enlarged phononic dispersion curves and phonon spectrum in the frequency region around phononic gap 3. The blue lines in parts (a,c) and the blue dots in parts (b,d) denote hinge vibrational modes.

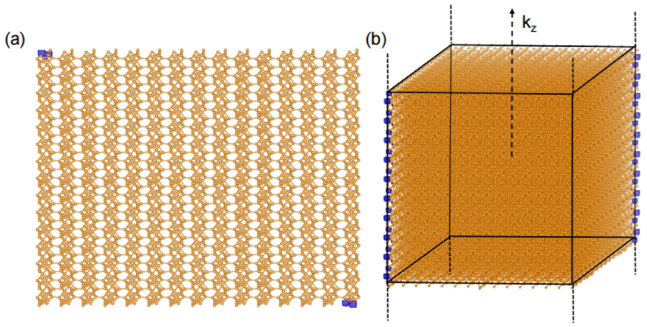

Figure 3. Spatial distributions for the doubly degenerate state at $k_z = 0$ (see Figure 2c,d) under (a) top and (b) side viewpoints.

Table 2. Parity Information of 3D 4^3T57-CA at the Four TRIM Λ_i Points

	Γ	X	M	Y
$N_3^+(\Lambda_i)$	12	14	13	13
$N_3^-(\Lambda_i)$	14	12	13	13
w_2	1			

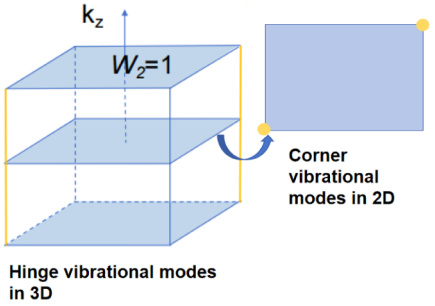

Figure 4. Schematic figure of corner vibrational modes in the 2D system and hinge vibrational modes for the 3D system.

(yellow dots) located at a pair of *PT*-related corner vibrational modes. These corner vibrational states constitute a pair of *PT*-related hinge vibrational modes for the 3D phononic SW insulator.

SUMMARY

To summarize, we demonstrated that the 3D 4^3T57-CA material has the potential to be a 3D phononic SW insulator. The phononic dispersion curves of 3D 4^3T57-CA can be experimentally measured using techniques such as inelastic neutron scattering or X-ray scattering spectroscopy. The w_2 for each k_z-slice of the BZ can characterize the bulk gap of the 3D SW insulator. The nontrivial phononic SW topology of the bulk 4^3T57-CA is also evident in the hinge vibrational modes, which exist throughout the 1D BZ. These hinge vibrational modes can be excited by infrared light at resonant frequencies and detected using local probes such as scanning tunneling microscopy. Phonon structure is another platform for the realization of second-order topological insulators. The phononic boundary states may be used for frequency filtering or mechanical energy attenuation under imperfect conditions, for heat transfer, and for infrared photoelectronics.[32] Our findings significantly expand the range of materials that can be considered as 3D phononic SW insulators and offer valuable guidance for further exploration of the phononic SW topology in 3D.

ASSOCIATED CONTENT

Supporting Information

The Supporting Information is available free of charge at https://pubs.acs.org/doi/10.1021/acsomega.4c08904.

Thermally and mechanically stable for 3D 4^3T57-CA (PDF)

AUTHOR INFORMATION

Corresponding Author

Yang Li − *Aviation and Automobile School, Chongqing Youth Vocational & Technical College, Chongqing 400044, China; College of Physics, Chongqing University, Chongqing 400044, China;* orcid.org/0000-0003-1059-356X; Email: liyang@cqwu.edu.cn

Complete contact information is available at: https://pubs.acs.org/10.1021/acsomega.4c08904

Notes

The author declares no competing financial interest.

https://doi.org/10.1021/acsomega.4c08904
ACS Omega 2024, 9, 46610−46614

■ ACKNOWLEDGMENTS

This work is supported by the Science and Technology Research Program of the Chongqing Municipal Education Commission (Grant No. KJZD-K202104101).

■ REFERENCES

(1) Wang, J.; Zhang, S. C. Topological states of condensed matter. *Nat. Mater.* **2017**, *16* (11), 1062−1067.
(2) Zhang, C.; Lu, H. Z.; Shen, S. Q.; Chen, Y. P.; Xiu, F. Towards the manipulation of topological states of matter: a perspective from electron transport. *Sci. Bull.* **2018**, *63* (9), 580−594.
(3) Wen, X. G. Choreographed entanglement dances: Topological states of quantum matter. *Science* **2019**, *363* (6429), No. eaal3099.
(4) Senthil, T. Symmetry-protected topological phases of quantum matter. *Annu. Rev. Condens. Matter Phys.* **2015**, *6* (1), 299−324.
(5) Song, Z.; Huang, S. J.; Qi, Y.; Fang, C.; Hermele, M. Topological states from topological crystals. *Sci. Adv.* **2019**, *5* (12), No. eaax2007.
(6) Massey, W. S. On the Stiefel-Whitney classes of a manifold. *Am. J. Math.* **1960**, *82* (1), 92−102.
(7) Kahn, B. The total Stiefel-Whitney class of a regular representation. *J. Algebra* **1991**, *144* (1), 214−247.
(8) Pan, M.; Li, D.; Fan, J.; Huang, H. Two-dimensional Stiefel-Whitney insulators in liganded Xenes. *Npj Comput. Mater.* **2022**, *8* (1), 1.
(9) Takahashi, R.; Ozawa, T. Bulk-edge correspondence of Stiefel-Whitney and Euler insulators through the entanglement spectrum and cutting procedure. *Phys. Rev. B* **2023**, *108* (7), 075129.
(10) Ahn, J.; Park, S.; Kim, D.; Kim, Y.; Yang, B. J. Stiefel−Whitney classes and topological phases in band theory. *Chin. Phys. B* **2019**, *28* (11), 117101.
(11) Wang, J. T.; Liu, J. X.; Ding, H. T.; He, P. Proposal for implementing Stiefel-Whitney insulators in an optical Raman lattice. *Phys. Rev. A* **2024**, *109* (5), 053314.
(12) Pan, M.; Huang, H. Phononic Stiefel-Whitney topology with corner vibrational modes in two-dimensional Xenes and ligand-functionalized derivatives. *Phys. Rev. B* **2022**, *106* (20), L201406.
(13) Qian, S.; Liu, C. C.; Yao, Y. Second-order topological insulator state in hexagonal lattices and its abundant material candidates. *Phys. Rev. B* **2021**, *104* (24), 245427.
(14) Zhou, H.; Zhang, G.; Zhang, Y. W. Effects of localized phonons on interfacial thermal conductance. *Phys. Rev. B* **2022**, *106* (19), 195435.
(15) Zhang, Z.; Ouyang, Y.; Cheng, Y.; Chen, J.; Li, N.; Zhang, G. Size-dependent phononic thermal transport in low-dimensional nanomaterials. *Phys. Rep.* **2020**, *860*, 1−26.
(16) Wang, X.; Yang, T.; Cheng, Z.; Surucu, G.; Wang, J.; Zhou, F.; Zhang, G.; Zhang, G. Topological nodal line phonons: Recent advances in materials realization. *Appl. Phys. Rev.*, **2022**, *9*, 4. .
(17) Jung, Y.; Lee, W.; Han, S.; Kim, B. S.; Yoo, S. J.; Jang, H. Thermal transport properties of phonons in halide perovskites. *Adv. Mater.* **2023**, *35* (43), 2204872.
(18) Spann, B. T.; Weber, J. C.; Brubaker, M. D.; Harvey, T. E.; Yang, L.; Honarvar, H.; Bertness, K. A.; Treglia, A. C.; Lee, M.; Hussein, M. I.; Bertness, K. A. Semiconductor thermal and electrical properties decoupled by localized phonon resonances. *Adv. Mater.* **2023**, *35* (26), 2209779.
(19) Taneja, V.; Das, S.; Dolui, K.; Ghosh, T.; Bhui, A.; Bhat, U.; Biswas, K.; Pal, K.; Datta, R.; Biswas, K. High Thermoelectric Performance in Phonon-Glass Electron-Crystal Like $AgSbTe_2$. *Adv. Mater.* **2024**, *36* (6), 2307058.
(20) Lu, G.; Pan, Z.; Gubbin, C. R.; Kowalski, R. A.; De Liberato, S.; Li, D.; Caldwell, J. D. Launching and manipulation of higher-order in-plane hyperbolic phonon polaritons in low-dimensional heterostructures. *Adv. Mater.* **2023**, *35* (22), 2300301.
(21) Zhang, L.; Ren, J.; Wang, J. S.; Li, B. Topological nature of the phonon Hall effect. *Phys. Rev. Lett.* **2010**, *105* (22), 225901.
(22) Ding, Z. K.; Zeng, Y. J.; Liu, W.; Tang, L. M.; Chen, K. Q. Topological Phonons and Thermoelectric Conversion in Crystalline Materials. *Adv. Funct. Mater.* **2024**, *34* (33), 2401684.
(23) Liu, Y.; Zou, N.; Zhao, S.; Chen, X.; Xu, Y.; Duan, W. Ubiquitous topological states of phonons in solids: Silicon as a model material. *Nano Lett.* **2022**, *22* (5), 2120−2126.
(24) Qin, P.; Liu, G.; Wu, P.; Xu, H. Diverse degeneracy types in topological phonons: A perspective. *Appl. Phys. Lett.*, **2024**, *124*, 3. .
(25) Liu, Y.; Chen, X.; Xu, Y. Topological phononics: from fundamental models to real materials. *Adv. Funct. Mater.* **2020**, *30* (8), 1904784.
(26) Li, J.; Kuang, M.; Bai, J.; Ding, G.; Yuan, H.; Xie, C.; Wang, X.; Wang, X. Coexistence of magnetic and phononic second-order topological phases in two-dimensional $NiZrCl_6$. *Appl. Phys. Lett.*, **2023**, *123*, 1. .
(27) Mu, H.; Liu, B.; Hu, T.; Wang, Z. Kekulé lattice in graphdiyne: Coexistence of phononic and electronic second-order topological insulator. *Nano Lett.* **2022**, *22* (3), 1122−1128.
(28) Zhu, J.; Wu, W.; Zhao, J.; Chen, C.; Wang, Q.; Sheng, X. L.; Yang, S. A.; Zhao, Y. X.; Yang, S. A. Phononic real Chern insulator with protected corner modes in graphynes. *Phys. Rev. B* **2022**, *105* (8), 085123.
(29) Li, J.; Liu, Y.; Bai, J.; Xie, C.; Yuan, H.; Cheng, Z.; Zhang, G. Phononic Weyl pair, phononic Weyl complex, phononic real Chern insulator state, and phononic corner modes in 2D Kekulé-order graphene. *Appl. Phys. Rev.* **2023**, *10* (3), 030416.
(30) Blatov, V. A.; Yang, C.; Tang, D.; Zeng, Q.; Golov, A. A.; Kabanov, A. A. High-throughput systematic topological generation of low-energy carbon allotropes. *Npj Comput. Mater.* **2021**, *7* (1), 15.
(31) Xue, H.; Chen, Z. Y.; Cheng, Z.; Dai, J. X.; Long, Y.; Zhao, Y. X.; Zhang, B. Stiefel-Whitney topological charges in a three-dimensional acoustic nodal-line crystal. *Nat. Commun.* **2023**, *14* (1), 4563.
(32) Xu, Y.; Vergniory, M. G.; Ma, D. S.; Mañes, J. L.; Song, Z. D.; Bernevig, B. A.; Elcoro, L.; Elcoro, L. Catalog of topological phonon materials. *Science* **2024**, *384* (6696), No. eadf8458.
(33) Chen, C.; Wu, W.; Yu, Z. M.; Chen, Z.; Zhao, Y. X.; Sheng, X. L.; Yang, S. A. Graphyne as a second-order and real Chern topological insulator in two dimensions. *Phys. Rev. B* **2021**, *104* (8), 085205.
(34) Wang, J.; Zhang, T. T.; Zhang, Q.; Cheng, X.; Wang, W.; Qian, S.; Wang, X.; Zhang, G.; Wang, X. 3D Carbon Allotropes: Topological Quantum Materials with Obstructed Atomic Insulating Phases, Multiple Bulk-Boundary Correspondences, and Real Topology. *Adv. Funct. Mater.* **2024**, *34* (30), 2316079.
(35) Gong, J.; Wang, Y.; Han, Y.; Cheng, Z.; Wang, X.; Yu, Z. M.; Yao, Y. Hidden Real Topology and Unusual Magnetoelectric Responses in Two-Dimensional Antiferromagnets. *Adv. Mater.* **2024**, *36* (29), 2402232.
(36) Wang, Y.; Cui, C.; Zhang, R. W.; Wang, X.; Yu, Z. M.; Liu, G. B.; Yao, Y. Mirror real Chern insulator in two and three dimensions. *Phys. Rev. B* **2024**, *109* (19), 195101.
(37) Zhang, X.; He, T.; Liu, Y.; Dai, X.; Liu, G.; Chen, C.; Yang, S. A. Magnetic Real Chern Insulator in 2D Metal−Organic Frameworks. *Nano Lett.* **2023**, *23* (16), 7358−7363.
(38) Wang, X.; Li, X. P.; Li, J.; Xie, C.; Wang, J.; Yuan, H.; Zhang, G.; Cheng, Z.; Yu, Z.-M.; Zhang, G. Magnetic second-order topological insulator: an experimentally feasible 2D CrSiTe3. *Adv. Funct. Mater.* **2023**, *33* (49), 2304499.
(39) Kresse, G.; Furthmüller, J. Efficient iterative schemes for ab initio total-energy calculations using a plane-wave basis set. *Phys. Rev. B* **1996**, *54* (16), 11169.
(40) Hammer, B. H. L. B.; Hansen, L. B.; Nørskov, J. K. Improved adsorption energetics within density-functional theory using revised Perdew-Burke-Ernzerhof functionals. *Phys. Rev. B* **1999**, *59* (11), 7413.
(41) Perdew, J. P.; Burke, K.; Ernzerhof, M. Generalized gradient approximation made simple. *Phys. Rev. Lett.* **1996**, *77* (18), 3865.
(42) Togo, A. First-principles phonon calculations with phonopy and phono3py. *J. Phys. Soc. Jpn.* **2023**, *92* (1), 012001.

https://doi.org/10.1021/acsomega.4c08904
ACS Omega 2024, 9, 46610−46614

(43) Hoffmann, R.; Kabanov, A. A.; Golov, A. A.; Proserpio, D. M. Homo citans and carbon allotropes: for an ethics of citation. *Angew. Chem., Int. Ed.* **2016**, *55* (37), 10962−10976.
(44) Ma, F.; Jiao, Y.; Jiang, Z.; Du, A. Rhombohedral lanthanum Manganite: a new class of Dirac half-metal with promising potential in spintronics. *ACS Appl. Mater. Interfaces* **2018**, *10* (42), 36088−36093.
(45) Born, M.; Huang, K. *Dynamical Theory of Crystal Lattices*; Clarendon Press: Oxford, 1954.
(46) *The PhononpyTB only needs the POSCAR and FORCE_CONSTANTS files to generate the phonon TB model. For* 4^3*T57-CA, we first calculated the phonon dispersion, and then constructed the TB model directly via the following command: python phonon_hr.py -d − dim = "2 2 2" -c POSCAR -p band.conf, where dim = "2 2 2" is just for a supercell with 2*2*2 size*. 2023, https://github.com/quanshengwu/wannier_tools/blob/master/utility/phonopyTB/phonon_hr.py.
(47) Pu, Z.; He, H.; Luo, L.; Ma, Q.; Ye, L.; Ke, M.; Liu, Z. Acoustic higher-order Weyl semimetal with bound hinge states in the continuum. *Phys. Rev. Lett.* **2023**, *130* (11), 116103.
(48) Choi, Y.-B.; Xie, Y.; Chen, C.-Z.; Park, J.; Song, S.-B.; Yoon, J.; Kim, B. J.; Taniguchi, T.; Watanabe, K.; Kim, J.; Fong, K. C.; et al. Evidence of higher-order topology in multilayer WTe_2 from Josephson coupling through anisotropic hinge states. *Nat. Mater.* **2020**, *19* (9), 974−979.
(49) Cheng, X.; Chen, J.; Zhang, L.; Xiao, L.; Jia, S. Antichiral edge states and hinge states based on the Haldane model. *Phys. Rev. B* **2021**, *104* (8), L081401.
(50) Zeng, X. T.; Chen, Z.; Chen, C.; Liu, B. B.; Sheng, X. L.; Yang, S. A. Topological hinge modes in Dirac semimetals. *Front. Phys.* **2023**, *18* (1), 13308.
(51) Zeng, X. T.; Liu, B. B.; Yang, F.; Zhang, Z.; Zhao, Y. X.; Sheng, X. L.; Yang, S. A. Three-dimensional real Chern insulator in bulk γ-graphyne. *Phys. Rev. B* **2023**, *108* (7), 075159.

https://doi.org/10.1021/acsomega.4c08904
ACS Omega 2024, 9, 46610−46614